#192 #192

FERMILAB-PUB-73-141-E

(To be submitted to Nucl. Instr. and Methods)

HEPL 677

NAL-75

OCTOBER, 1972

Copies to Rand - Peoples - Nash

How about fuzzing of electron optics by [illegible]

Probably pretty small effect

ELG

A HIGH QUALITY ELECTRON/PHOTON BEAM FOR NAL*

Z. G. T. Guiragossián and R. E. Rand

High Energy Physics Laboratory

W. W. Hansen Laboratories of Physics

Stanford University

Stanford, California 94305

* Work supported by the National Science Foundation, Grant No. GP 28299

Proposal File No. ~~[illegible]~~ 192
Master
DO
JRS

ABSTRACT

A design for a secondary electron beam suitable for electron scattering experiments at the National Accelerator Laboratory is presented. Using standard NAL beam transport magnets it will operate at up to 300 GeV/c with the following properties: Acceptance 9.5 μster % $\Delta p/p$ (FW), momentum bite ± 2% , momentum resolution of momentum hodoscope $\Delta p/p$ = ± 0.30% (HW at base), final spot size $\leq$ ± 3.0 mm × ± 5.5 mm (HW at base). Hodoscopes are also included for measuring the angles at which electrons pass through the experimental target with resolutions in both planes of better than ± 0.1 mr. These properties are achieved by a periodic beam structure which includes correction of second order aberrations by means of sextupoles. The yield of electrons is estimated to be $\sim 10^8/10^{13}$ incident protons when the energy of the electrons is about one half the energy of the protons. It is emphasized that synchroton radiation by electrons in the beam transport magnets is very significant in reducing pion contamination of the final beam spot. It is shown that superconducting magnets to enhance this effect are superfluous. Pion impurity is $\leq$ 0.01% at every energy and may be made essentially zero at energies greater than 160 GeV. The beam is designed with four focussing stages, the first two of which provide a beam spot of sufficient quality for tagged photon experiments.

I. INTRODUCTION

The electron scattering experiments proposed[1] at the National Accelerator Laboratory require an electron beam of high purity with very fine energy and angular resolution. At the same time it is important that these qualities are not achieved at the expense of electron intensity, a valuable commodity at NAL. The beam must also be compatible with providing a tagged photon facility for which the electron beam specification is not so stringent. It has been suggested[2] that to meet these requirements, the beam should be constructed in two phases, the first of which (2 stages) would provide the photon beam while the second phase (total 4 stages) would constitute the high quality electron beam. The present design meets these requirements which are translated into quantitative terms in section 2 and Table I. Figure 1 shows a schematic layout of the beam. The functions[3] of the 4 focussing stages are as follows:

(1) Electron production [protons produce π^0's in primary target of low Z material: Be or deuterium, (Be is used for practical reasons), sweeping magnets remove protons and other charged particles from neutral stage of beam; photons from π^0 decays pair-produce electrons in a high Z radiator, (Pb or U)], primary defining apertures, horizontally (x) dispersed focus (F1) to define momentum bite cleanly, vertical (y) focus ($F\frac{1}{2}$) with slit to reduce π^- contamination. (The primary target is the virtual object of the beam optics.)

(2) Magnet after F1 to clean up beam, achromatic focus at F2. This focus is used for the tagged photon beam (Phase I) or with a horizontal slit to further eliminate pions in the 4 stage beam (Phase II).

(3) Dispersed focus at F3 with momentum hodoscope.

(4) Angle hodoscopes at first foci of last set of quadrupoles. These measure directly the angles (θ horiz., ϕ vert.) at which an electron passes through the experimental target located at the achromatic focus F4.

The beam is designed for a maximum momentum of 300 GeV/c. Careful attention was paid to the desirability of using standard NAL transport magnets throughout. Components are described in Table II.

II. SPECIFICATION OF BEAM QUALITY

In order for the electron beam to be suitable for scattering experiments, it is essential that it meet the following specifications which result from a realistic assessment of the experimental requirements and possible beam performance.

(a) Beam intensity of $\sim 10^8$ electrons/pulse from 10^{12} - 10^{13} incident protons, requiring[4] an acceptance of at least 8 μster % $\Delta p/p$ (full width). In practice this means $\Delta p/p \simeq 4\%$ (FW) and $\Delta\Omega \simeq 2$ μsterad.

(b) Maximum momentum 300 GeV/c.

(c) Well defined momentum bite, i.e. momentum resolution at the first dispersed focus (F1), $\Delta p/p \leq \pm 0.5\%$ at base of distribution.

(d) Momentum resolution at third focus (F3), $\Delta p/p \leq \pm 0.3\%$ at base of distribution.

(e) Momentum hodoscope at F3 to take full advantage of this resolution.

(f) Angle measuring hodoscopes (both planes) in the last stage with a resolution of $\leq$ 0.1 mrad.

(g) Achromatic beam spot at final focus F4 $\leq \pm 2.5$ mm $\times \leq \pm 7.5$ mm at base of distribution.

(h) Low energy contamination (halo) of final beam spot < 0.001 %.

(i) Electron purity: π/e ratio $\leq 3 \times 10^{-4}$ (Pions are produced by neutrons which interact in the Pb/U radiator). It is emphasized that electron purity is strongly influenced by the optical quality of the beam design, since electrons lose energy by synchrotron radiation throughout the beam transport system and thus may be separated from pions provided that the final beam spot is small and free from aberrations. μ/e ratio $\leq 10^{-6}$ (Muons from pion decay and other sources are transmitted mainly through the earth shielding of the beam which is about 5 meters below ground level).

(j) Suitable optics (achromatic beam spot and space which could accomodate the photon tagging apparatus at the second focus (F2). Here the electron purity is not so critical and no beam hodoscopes are required before this point. The specification for a tagged photon beam has been discussed by Halliwell et al.[5)]

The following sections describe a design which meets this specification.

III. ELECTRON PRODUCTION

The design of a "front end" or electron production stage has been fully discussed elsewhere.[5)] The parameters of this part of the beam are largely dictated by necessary functions and little freedom is available for variations in design. The main components are illustrated in the schematic layout, Fig. 1, and discussed below.

The angle of incidence of the proton beam at the primary target may be varied by a set of bending magnets. This enables one to use production angles other than 0°, so that, at the sacrifice of some intensity, one may

improve the final π/e ratio if at all necessary. The primary target itself should be of a material which maximises the ratio of π^o production to photon attenuation. Deuterium is the optimum choice for this condition but for practical reasons would probably not be used. Beryllium is the most reasonable alternative. There is an optimum target thickness for which the maximum number of photons (from π^o) are produced. This thickness is ~ 1.13 interaction lengths for beryllium as shown below. The n/γ ratio (π^-/e ratio) decreases monotonically with target thickness but is expected to be sufficiently small at this optimum thickness.

An estimate of the electron yield to be expected is made as follows. Recent results from the ISR show[6] that the cross section for inclusive π^o production from pp collisions is equal to the average of the cross sections for π^- and π^+. The latter have been measured at BNL and CERN and are well described by a multiperipheral model.[7] This model has been used to calculate π^o production and hence the electron yield to be expected.

The number of decay photons from π^o's produced in the target is obtained by integrating:

$$\frac{dN_\gamma(k)}{dk\, d\Omega} = 2\int_k^{p_o} \frac{T}{\lambda} \frac{\epsilon}{\sigma_a(pp)} \frac{d\sigma_{\pi^o}}{dp_{\pi^o} d\Omega} \frac{dp_{\pi^o}}{p_{\pi^o}}$$

where T = target length,

λ = hadronic interaction length in the target

$$\epsilon = \frac{1}{T}\left[\frac{\exp\left(-\frac{7}{9}\frac{T}{x_o}\right) - \exp\left(-\frac{T}{\lambda}\right)}{\frac{1}{\lambda} - \frac{7}{9}\frac{1}{x_o}}\right]$$ is an effective target efficiency,

x_o = radiation length in the target

$\sigma_a(pp)$ = 31 mb[8] (absorption cross section)

p_o, p_{π^o} = proton and π^o momenta

and the differential cross section is obtained from

$$\frac{d\sigma_{\pi^o}}{dp_{\pi^o}d\Omega} = \frac{1}{2}\left[\frac{d\sigma_{\pi^-}}{dp\ d\Omega} + \frac{d\sigma_{\pi^+}}{dp\ d\Omega}\right]$$

The target efficiency is maximised at an optimum target length of $\frac{T}{\lambda} = \frac{c}{c-1}\ \ell nc$, where $c = \frac{9}{7}\frac{x_o}{\lambda}$. Using the measured[9] value of λ = 35.7 cm for beryllium and x_o = 35.7 cm, one obtains $\frac{T}{\lambda} \doteq 1.13$, i.e. T = 40.3 cm.

This formula gives an exact energy spectrum for the photons because of the isotopic decay distribution in the π^o center of mass. But the angular distribution of photons is approximate since only the π^o production angle is included. The approximation is good to angles of order m_{π^o}/E_{π^o}. It is assumed that production of photons by other processes is negligible.

Between the primary and secondary targets a set of 4 bending magnets (13.1 m × 14 kg) separate the protons and other charged particles from the neutral components of the beam. This is sufficient to handle primary momenta up to 500 GeV/c. The proton beam is dumped in the vicinity of the first electron beam quadrupole, below the beam line level.

The second target or radiator consists of a high Z material such as lead or uranium which has a high ratio of collision length to radiation length. Elsewhere[5] it has been shown by a Monte Carlo calculation

that the optimum thickness for the radiator is approximately 0.5 radiation lengths. The yield of electrons is now obtained from the approximate formula.[10)]

$$\frac{dN_e(p)}{dp\ d\Omega} \simeq \left[1 - \exp\left(-\frac{7}{9} \cdot \frac{\ell}{x_o}\right)\right] \int_p^{p_o} \frac{dN_\gamma(k)}{dk\ d\Omega} \frac{dk}{k}$$

where ℓ is the radiator thickness.

The position of the secondary target or radiator is not critical but should be as close to the primary target as possible. This will minimise the effective source size at the primary target, due to multiple scattering of electrons in the radiator. A primary to secondary target separation of 22.8 m is chosen.

In Figs. 2(a) - 2(e) are shown the calculated electron yields for the present beam design and for primary proton momenta of 200, 300, 400 500 and 1000 GeV/c respectively. The dependence of the yield on production angle is also shown. It is evident that the energy of the primary proton beam is a more important factor than the intensity. For example, 10^{12} protons/ pulse at 400 GeV/c produce more high energy electrons than 10^{13} protons/pulse at 200 GeV/c.

IV. ELECTRON BEAM OPTICS

It would be impossible to meet the specifications detailed in section II without correcting the main chromatic aberrations in the beam. Any beam design of this length (600 m) and moderately large acceptance, with magnetic elements of no higher order than quadrupole, would be expected to suffer from second order chromatic aberrations of several times first order effects. From the start, the beam optics were designed therefore to be compatible with sextupole correction of second order terms.

This feature is essential to the proposed electron scattering experiments for without it, it would not be possible to achieve the necessary momentum and angular resolutions and especially the small spot size and high electron purity. The latter parameter is directly affected by the size of the electron beam envelope at F2 where a horizontal collimator is used to define a pion spot. This feature is important not only because it removes pions from the beam at F2, but because it enhances the π-e separation at F4, caused by synchrotron radiation by electrons in the beam bending magnets.

Experience has shown that sextupole magnets can only be successfully used in a beam line by locating them as optically conjugate pairs with equal strengths, i.e. the transfer matrix between the sextupoles must be identically $\pm$ unity. This ensures that even order geometrical aberrations introduced by the sextupoles cancel outside the pairs. Sextupole pairs cannot be interlaced without introducing serious third order aberrations. For each pair, the strength can be chosen to cancel exactly only one second order chromatic aberration of the beam. (Higher multipole magnets are not considered here). These conditions imply that the number of stages between fully corrected foci in a beam line must be at least two for correction in one plane and three for both planes. Exact correction of the electron beam is not therefore possible, but the following acceptable compromise has been attained. The design is based on the exact correction of the main chromatic aberration term $\langle x | x_o' \delta \rangle$ [11] in the horizontal bending plane (x) at F2 and F4. This is done in such a way that the geometric aberrations (mainly $\langle x | x_o' \, x_o' \rangle$ inevitably introduced at F1 and F3 are tolerable. Worsening of the chromatic aberration in y is avoided by locating the sextupoles at y foci where they have negligible effect. A small spot size in y at each x focus (between the true y foci) is obtained by locating an angle

focus waist ($< y | y_o > = < y' | y'_o > = 0$) at these positions. This arrangement also ensures that chromatic aberrations in y at all x foci are negligible. (There are aberrations in y' however).

The first y focus, where pions are removed from the beam, is therefore inside the first stage ($F\frac{1}{2}$) where chromatic aberrations are small. Location of the sextupole pairs at conjugate points requires that the beam-structure be periodic from $F\frac{1}{2}$ to $F3\frac{1}{2}$. However, the design of the first quadrupole doublet need not form part of this structure and has been chosen to produce a magnification in the first stage of 2.4 in x and 3.0 in y. This increases the acceptance of the periodic part of the beam and enables one to use a reasonable focal length for the quadrupoles (24.4m). It also helps to reduce the geometric aberration introduced by the first sextupole at F1 and the third at F3. Similarly the last half of the last stage ($F3\frac{1}{2}$ - F4) does not form part of the periodic structure and is designed purely to obtain the required beam spot size and to provide suitable locations for the θ and ϕ hodoscopes.

At the sextupoles the dispersions $< x | \delta >$ are equal and optimized so that $< x | x'_o > x'_o$ is just less than $2 < x | \delta > \delta$ where $\delta \equiv \Delta p/p$. This ensures that the acceptance is maximized, the sextupole strength is minimised and that the geometric aberrations at F1 and F3 are much less than the original chromatic aberrations at F2 and F4. This condition also implies, however, that $< x | x'_o > x'_o$ is only 2/3 of the available aperture. Hence the use of sextupoles inevitably leads to a reduction in acceptance. This arrangement is also a compromise between correcting $< x | x'_o \delta >$ at F1 and F3 (which requires $< x | \delta >$ at the odd sextupoles greater than $< x | \delta >$ at the even ones)and correcting $< x | \delta\delta >$ at F2 and F4 (which requires the

opposite). Even so these terms are not significant.

Magnet positions and strengths were calculated using the computer program TRANSPORT[12]. Rays were traced through the final system, using the program TURTLE[13] to evaluate the performance of the beam transport and the effect of synchrotron radiation by electrons. The performance which appears to satisfy all electron scattering and tagged photon experiment requirements is shown in Table I. Also shown there are the electron yields caclulated both by the method outlined in section III and by a Monte Carlo calculation[14] based on the Hagedorn-Ranft model. π/e ratios are also based on this model, but depend strongly on the effects of synchrotron radiation described in section V. Magnetic components of the beam are listed in Table II.

Figure 3 shows the layout of the beam, the TRANSPORT matrix elements and beam envelopes.

Figures 4-9 show TURTLE generated histograms at the various foci both with and without sextupole correction. These results are correct to all orders in the optics. Calculations were performed with an effective primary electron spot size of ± 2.5 mm in both planes, the value expected at 100 GeV/c . The main effect contributing to this spot size is multiple scattering in the radiator. A primary aperture slit of $x = \pm 15$ mm and $y = \pm 30$ mm at the first quadrupole is used in all calculations. However the acceptance (9.5 μster % $\Delta p/p$ FW) quoted in Table I is for a y slit of ± 37.5 mm. The only effect of this larger slit is to increase the vertical spot sizes at F2 and F4 proportionally. It causes no significant change in beam losses or purity.

Imperfections in the quadrupole fields as found in actual measurements[15] were included in the ray tracing calculations by using a higher order multipole expansion. It is interesting to note that in this type of periodic beam structure, such imperfections have virtually no effect because of cancellations at conjugate lens positions.

Figure 4 shows the vertical beam profile at the first y focus where a slit is used to effect the primary removal of pions from the beam. Pions, which are generated mostly by neutrons in the lead radiator, are produced with a much greater spread of angles than are electrons so that the effective pion spot size at the primary target is much larger than that for electrons as shown in Table I. The π/e ratio in the whole beam may therefore be improved by locating "scrapers" or slits at the x and y foci. The π/e ratio at F2 quoted in Table I is the value obtained after vertical scraping at $F\frac{1}{2}$, only. Horizontal slits at F2 serve to further improve this ratio at F4 as described in section V. Very few electrons are lost at these scrapers.

The momentum resolution and acceptance at the first dispersed focus F1 are shown in Fig. 5. Here the slight asymmetry of the beam profiles due to the geometric aberrations introduced by the single sextupole SX1 may be seen. The resolution is sufficient to ensure a very sharp cutoff of the momentum spectrum.

Figure 6 shows the beam profiles at the achromatic focus F2 where tagged photon experiments may be performed. Sextupole correction of the chromatic aberrations at this point is seen to be essential to the subsequent properties of the beam. In the region of F2, the beam envelope (with quadrupoles 11 and 12 omitted) is confined to ± 12.5 mm in both dimensions over a length of 50 m at 100 GeV/c. At higher momenta it is narrower still. This condition

is adequate for several tagged photon experiments.[16] More complex spot requirements[17] have been obtained by the addition of two extra quadrupoles on either side of bending magnets 11 and 12.

The momentum resolution at F3 is shown in Fig. 7. This may be slightly improved by an appropriate slit at F2 as shown in Table I without significant loss of intensity. The centroid displacement for the rays of nominal momentum (p_o) is due mainly to the transport matrix element $< x | x_o' \; x_o' >$ while at 1.016 p_o additional effects due to $< x | \delta\delta >$ are seen. This implies that the momentum hodoscope calibration will not be exactly linear.

The angular resolutions at the angle hodoscopes are shown in Fig. 8 and numerically in Table I. Inspite of the impossibility of placing the θ hodoscope where the dispersion is exactly zero and the ϕ hodoscope exactly at the appropriate focus, the intrinsic angular resolutions are easily adequate for the experimental requirements. Greater spread is introduced by the finite size of the hodoscope elements (section VI).

Finally Figs. 9 and 10 show the electron and pion beam profiles at F4 where the experimental target will be located. The spot sizes easily satisfy the experimental requirements. The separation of the electron and pion beam spots by synchrotron radiation is discussed below (section V).

An important property in a secondary electron beam is cleanness in momentum. That is, it should not be possible for a significant number of electrons with momenta outside the nominal limits to pass through the experimental beam spots at F2 and F4. The periodic beam structure described here performs well in this respect. Between F1 and F2, only 0.3% of the electrons are lost. Furthermore, it is impossible for electrons of momenta

less than $0.865\ p_o$ to pass through the beam spot at F2. In stage 4, losses only occur (inevitably) at the hodoscope. In each case it is possible to place a veto shower counter where it may detect photons radiated by an electron in the hodoscope elements as discussed in section VI.

V. ELECTRON BEAM PURITY AND SYNCHROTRON RADIATION

The permissibile level of pion contamination of the electron beam is determined primarily by the pion rejection capability of the experimental electron detectors. A secondary consideration is that in a 25 cm liquid hydrogen target for instance, 1.4% of all interacting pions would produce electrons via π^o production followed by $\pi^o \rightarrow \gamma\gamma$ and $\gamma \rightarrow e^+e^-$. These electrons are produced mainly at low energies and do not constitute a significant background.

The electron detectors[1)] under development in this laboratory consist of several large NaI(Tl) crystals interleaved with multi-wire proportional chambers. Tests with these detectors have shown that at 10 GeV, the probability of a pion being identified as an electron is $< 0.3\%$ if the momentum is known to 3%. There is reason to expect this uncertainty to drop to 0.1% at NAL energies. Now the ratio of the total cross sections for $\pi^- p$ to $e^- p$ interactions is typically 10^3. Hence the probability of confusing a hadron from a π^- interaction, with a scattered electron is conservatively 0.09% for a π/e contamination ratio of 3×10^{-4}. Such a systematic error is certainly less than other experimental errors, systematic or statistical. The numbers in Tables I and III show that such an electron purity is attainable in the present beam design at the final focus F4. At F2, however, the pion contamination is unacceptable. The same would be true in a 4-stage beam not corrected for second order aberrations.

The flux of pions which remains within the electron beam spot at F4 depends on several factors, the most important of which are production mechanisms at the primary target, beam optics and synchrotron radiation. It has not been generally realized that this last effect - synchrotron radiation of electrons in the conventional beam bending magnets - is very significant.

This may be seen as follows. The fractional loss in momentum of an electron of energy E(GeV) passing through a uniform magnetic field B(kgauss) of length L (meters) is given by

$$\frac{\Delta p}{p} = 1.26 \times 10^{-8} \; E \, B^2 \, L$$

Hence for a 200 GeV electron in a field of 14 kgauss of length 3.05 m, $\Delta p/p = 0.15\%$. This is a small effect but the deviation due to this momentum loss is 4.8 μrad. Again this is a small angle but in each phase of the beam there are about 10 magnets with an average lever arm of ~ 100 m. Hence if the magnet settings are not compensated for this effect, the electron beam spot will be shifted ~ 5 mm, more than the total spot size. If however the magnet settings are "radiation compensated" as in Table II, the electron beam spot will be on axis with a separate pion beam spot off axis by ~ 5 mm. Thus the pion contamination can be reduced almost to zero (Table III) by a suitable scraper or veto counter.

This effect is illustrated by the beam profiles in Fig. 10 which are due to exact ray tracing calculations using the program TURTLE.

(The momentum and deviation of each ray were suitably offset after each bending magnet.) In Fig. 10 all beam profile distributions are normalized arbitrarily to have equal heights. The magnet settings used were those shown in Table II. At energies less than 300 GeV, magnet settings within each group of magnets are optional provided the integral $\int B d\ell$ is correct and B does not exceed 14 kgauss. They have been chosen as follows. For energies greater than 200 GeV, it is sufficient to use a minimum number of the available magnets with power distributed equally between them, to achieve almost complete separation of pions and electrons. At lower energies the effect of synchrotron radiation may be optimised by using all available magnets with reversed fields where necessary so that the integral $\int B^2 d\ell$ is maximized but the beam line geometry is preserved. This procedure is illustrated at 100 and 150 GeV in Table II and Fig. 10. It provides a substantial reduction in pion contamination which would become zero at about 160 GeV.

Synchrotron radiation will also be responsible for some reduction in beam quality due to the statistical fluctuations of the process. It is estimated that these effects will cause an additional beam spot spread of ~ 0.5 mm at F4 at ~ 200 GeV and a momentum spread of ~ 0.2%. Both of these figures make negligible contributions when folded quadratically with the respective geometrical values.

It has been suggested[18] that synchrotron radiation be used to enhance electron beam purity by placing a "chicane" of superconducting magnets at the intermediate focus of the beam (F2). Thus the electron momenta would be shifted by a large amount at this point and with the second phase of the beam tuned accordingly, pions could be eliminated. However it is now

seen that the distributed effect of synchrotron radiation along the beam line is sufficient to reduce pion contamination to an acceptable level in the present beam design and application.

The "chicane" thus appears to be of limited usefulness in this beam design. If, however, it is desired to produce a completely pure electron beam so that less discriminating detectors may be used in other experiments a superconducting chicane of 70 kgauss × 0.2 m would shift the electron momenta ~ 2% at 100 GeV, sufficient to cause all pions to be lost at F3. The device would be redundant above 160 GeV.

A more economical way of enhancing the electron beam purity consists of filtering out the neutron and K^o components at the neutral stage of the beam. This may be achieved by placing a liquid deuterium filter inside a bending magnet in front of the lead radiator. Such a filter 3.3 m long would remove 63% of the hadronic neutrals and transmit 72% of the photons. The pion contamination would thus be reduced by a factor of 2.0 to a level of $\pi/e \lesssim 10^{-5}$ at F4. The electron to hadron singles ratio in the detector would then be ~ 100:1 . A beryllium primary target followed by a deuterium filter would appear to be a more economical arrangement than a simple deuterium primary target.

Muons produced by decay of pions, and other processes from the primary target may cause some contamination of the electron beam especially at F2. These high energy muons are transmitted mainly through the earth shielding of the underground beam line. Calculations[19)] have shown however that in this design such contamination is negligible.

VI. BEAM INSTRUMENTATION

While specific details of beam instrumentation would be worked out under practical operating conditions, the general requirements may be defined as follows. Small high resolution multi-wire proportional chambers could be used at low intensities to obtain beam profiles at various locations during commissioning of the beam. At high intensities and during actual operation, these would be replaced by small traversing plastic scintillation counters, located especially at all x and y foci. Remotely controlled beam slits would be placed in front of the first quadrupole QP1 and at the foci: $F\frac{1}{2}$ and F2 .

To define the momenta and angles of electrons passing through the experimental target at F4, 8 or 16 element plastic scintillator hodoscopes would be set up at the appropriate locations as shown in Fig. 3. At beam rates of $> 10^8$/sec special timing techniques would be necessary in using these hodoscopes. It is suggested that selected events at the experiment itself could be used to generate a gate of about 10 nsec duration, during which the timing pulses from all hodoscope elements could be digitized in parallel. Currently available gated time digitizers have an inherent resolution of 400 psec. True coincidences would be recognized by means of an on-line computer.

Veto shower counters, to detect photons radiated by beam electrons at the p, θ and ϕ hodoscopes, should be placed next to the beam transport elements QP16, BM25 and QP20 respectively. These counters need not be large since it is only necessary, for instance, to detect photons of energy $k > 300$ MeV to maintain a momentum resolution of better than 0.3% at 100 GeV/c.

This mode of operation is possible since each hodoscope is followed by a bending magnet which sweeps the electron beam away from the veto counters. A "beam-halo" veto located just in front of F4 would also be necessary especially to discriminate against pions. Other veto counters would be placed along the beam as necessary. Calculations indicate that the main veto counter rates would not exceed 1% of the beam rate.

Finally in the third and fourth stages, the beam design includes two drift spaces of about 40 meters each which can accomodate beam pipes instrumented to operate as low pressure threshold Cerenkov counters. These counters would serve the important function of monitoring the pion contamination of the electron beam. They would also be essential if the system were used as a high quality hadron beam.

VII. CONCLUSIONS

It has been demonstrated in detail that it is possible to produce a very high quality electron beam from the new generation of proton accelerators operating at 400 to 500 GeV. Electron fluxes of more than 10^8/pulse with a beam spot only a few millimeters across are feasible. Furthermore, momenta and directions of the electrons passing through the target may be determined with good resolution and high beam purity is possible without special devices. Finally it should be pointed out that such a beam line will operate equally well for hadrons and will in fact constitute a very versatile facility.

VIII. ACKNOWLEDGEMENTS

The authors would like to thank the many people who have contributed to the successful completion of this design study. They are especially indebted to Dr. J. J. Murray and Professor D. D. Reeder who were their main inspiration. Thanks also are due to A. L. Read, K. L. Brown, T. Nash and D. Carey for many clarifying discussions and much practical help. Professor R. Hofstadter has provided much encouragement and guidance throughout this effort. Finally, the authors are grateful to Professor R. R. Wilson and Professor E. L. Goldwasser for their continuous interest and support.

TABLE I

ELECTRON BEAM PERFORMANCE

Optical properties are calculated using the program TURTLE.[13)]

Yield calculations are described in the text. See Figs. 3 - 9. (A 1 mm radius proton beam spot is assumed.)

Electron Beam Momentum	100 GeV/c	200 GeV/c	Experimental Requirements
Electrons: effective source size at F0	2.5 mm rad	1.5 mm rad	-
Pions: effective source size at F0	10.0 mm rad	0.7 mm rad	-
Acceptance: μster % Δp/p FW	9.5	9.5	≥ 8
Electron Yield at F4/10^{13} p at 500 GeV/c Multiperipheral model:	6.2×10^{8}	1.9×10^{8}	10^{8}
Hagedorn-Ranft model:	2.2×10^{8}	0.47×10^{8}	
π/e ratio at F2	6.0×10^{-4}	1.2×10^{-3}	
π/e ratio at F4[(a)]	1.0×10^{-4}	4.6×10^{-6}	3×10^{-4}
Momentum Bite at F1 (HW at base)	+ 2.4%, - 2.1%	+ 2.4%, - 2.1%	-
(HWHM)	+ 2.2%, - 1.9%	+ 2.2%, - 1.9%	± 2%
Momentum Resolution at F1 (HW at base)	± 0.39%	± 0.30%	≤ ± 0.5%
Momentum Resolution at F3 (HW at base)	± 0.30% (± 5 mm slit at F2)	± 0.26% (± 4 mm slit at F2)	≤ ± 0.3%
Spot Size at F2 (HW base)	± 6.0 mm × ±8.5 mm	± 3.8 mm × ± 8.5 mm	-
Spot Size at F4 (HW base)	± 3.0 mm × ±5.5 mm	± 2.0 mm × ± 5.5 mm	≤ ± 2.5 mm × ± 7.5
θ Resolution at θ hodoscope (HWHM)	± 0.035 mr	± 0.035 mr	≤ ± 0.1 mr
φ Resolution at φ hodoscope (HWHM)	± 0.027 mr	< ± 0.027 mr	≤ ± 0.1 mr

(a) Electron purity due to beam optics, production cross sections, and synchrotron radiation throughout the beam. See Table III for details.

TABLE II

BEAM LINE COMPONENTS AND MAGNET SETTINGS

The settings for electrons are Radiation Compensated. For electrons at 100 and 150 GeV/c, magnet settings are optimized to maximize ΣB^2 (with the limit $B \leq$ 14 kgauss.).

All quadrupoles (QP): 3.81 cm rad × 3.048 m long (NAL # 3-Q-120)
All bending magnets (BM): 1.905 cm gap × 3.048 m long (NAL # 5-1.5-120)
All sextupoles (SX): 5.08 cm rad × 0.762 m long (NAL # 4-S-30)

Component	Position Front End (m)	Field Values at Pole (kgauss)				
		300 GeV/c hadron beam	300 GeV/c electron beam	200 GeV/c electron beam	150 GeV/c electrons max ΣB^2	100 GeV/c electrons max ΣB^2
Radiator	22.8					
Aperture (± 15 mm × 37.5 mm)	30.0					
QP1, 2	30.48	- 6.564	- 6.564	- 4.376	- 3.282	- 2.188
QP3,4	37.19	5.402	5.402	3.601	2.701	1.801
BM 1	55.32	10.792	10.763	7.189	- 3.204	- 6.799
BM 2 } bend = .752°	58.67	"	"	"	13.983	13.987
BM 3	62.03	"	"	"	"	"
BM 4	65.38	"	"	"	- 3.204	- 6.799
QP 5	94.49	2.451	2.438	1.632	1.223	0.816
Y Slit (F $\frac{1}{2}$) (± 9.0 mm)	97.84					
SX1	97.84	2.308	2.296	1.536	1.151	0.768
QP 6	118.87	- 5.297	- 5.269	- 3.526	- 2.642	- 1.763
F 1	167.64					
QP 7	167.64	5.297	5.269	3.526	2.642	1.763
BM 5 } bend = .456°	170.99	13.042	12.947	8.676	6.504	4.339
BM 6	174.35	"	"	"	"	"
QP 8	192.02	- 5.297	- 5.249	- 3.522	- 2.641	- 1.762
BM 7 } bend = .630°	230.73	12.025	11.885	7.989	13.940	12.973
BM 8	234.09	"	"	"	- 9.920	-13.958
BM 9	237.44	"	"	"	13.940	12.973
QP 9	240.79	5.297	5.223	3.517	2.634	1.759
SX 2	244.15	2.308	2.275	1.532	1.147	0.766
BM 10 bend = .210°	245.21	12.025	11.845	7.981	5.978	3.992
QP 10	265.18	- 5.297	- 5.214	- 3.515	- 2.633	- 1.759
BM 11 } bend = .489°	278.74	14.000	13.748	9.390	6.957	4.647
BM 12	282.09	"	"	"	"	"
F 2 (γ expt)	313.94					

TABLE II (cont.)

BEAM LINE COMPONENTS AND MAGNET SETTINGS

The settings for electrons are Radiation Compensated. For electrons at 100 and 150 GeV/c, magnet settings are optimized to maximize ΣB^2 (with the limit $B \leq$ 14 kgauss.).

All quadrupoles (QP): 3.81 cm rad × 3.048 m long (NAL # 3-Q-120)
All bending magnets (BM): 1.905 cm gap × 3.048 m long (NAL # 5-1.5-120)
All sextupoles (SX): 5.08 cm rad × 0.762 m long (NAL # 4-S-30)

Component	Position Front End (m)	Field Values at Pole (kgauss)				
		300 GeV/c hadron beam	300 GeV/c electron beam	200 GeV/c electron beam	150 GeV/c electrons max ΣB^2	100 GeV/c electrons max ΣB^2
X slit	313.94	-	4.1 mm	4.1 mm	4.8 mm	6.1 mm
QP 11	313.94	5.297	5.190	3.510	2.631	1.758
QP 12	338.33	- 5.297	- 5.190	- 3.510	- 2.631	- 1.758
BM 13	359.30	12.589	12.267	0	13.872	12.509
BM 14	362.65	"	"	12.467	- 9.033	-13.911
BM 15 (bend = 1.320°)	366.00	"	"	"	13.872	13.911
BM 16	369.36	"	"	"	13.872	13.911
BM 17	372.71	"	"	"	- 9.033	-13.911
BM 18	376.06	"	"	0	13.872	12.509
QP 13	387.10	5.297	5.134	3.485	2.617	1.751
SX 3	390.45	1.580	1.531	1.039	9.781	0.522
QP 14	411.48	- 5.297	- 5.134	- 3.485	- 2.617	- 1.751
(Čerenkov Counter)	-					
F 3 (p hodoscope)	460.25					
QP 15	460.25	5.297	5.134	3.485	2.617	1.751
BM 19 (bend = .380°)	463.60	10.874	10.524	7.150	5.372	3.594
BM 20	466.95	"	"	"	"	"
QP 16	484.63	- 5.297	- 5.120	- 3.482	- 2.617	1.751
(Čerenkov Counter)	-					
ϕ Hodoscope	528.48					
BM 21 bend = .156°	528.98	8.925	8.622	5.865	4.408	2.950
SX 4	532.33	1.580	1.526	.1038	0.780	0.522
QP 17	533.40	6.829	6.594	4.488	3.366	2.257
BM 22	536.75	14.000	13.457	9.187	0	- 4.623
BM 23 (bend = .976°)	540.11	"	"	"	13.813	13.869
BM 24	543.46	"	"	"	"	"
BM 25	546.81	"	"	"	0	- 4.623
θ Hodoscope	550.62					
QP 18	551.38	- 7.000	-6.698	- 4.587	- 3.450	- 2.310
QP 19	554.74	- 2.899	-2.774	- 1.900	- 1.429	- 0.956
BM 26 bend = .244°	558.09	14.000	13.382	9.172	6.898	4.619
QP 20	568.36	7.000	6.683	4.584	3.449	2.310
F 4 (Electron expt)	577.51					
Final central momentum (GeV/c) -		300.0	286.4	196.5	147.8	99.0

TABLE III

π/e RATIOS AND EFFECTS OF SYNCHROTRON RADIATION

Energy GeV	Beam mode	π/e Ratio[a] after slit at F2	Fractions of pions[b] in e spot at F2 which remain in e spot at F4	π/e Ratio at F4	π/e Ratio with D_2 filter
300	all magnets	not available	0	0	0
200	min magnets	2.7×10^{-4} (c)	.017	4.6×10^{-6}	2.3×10^{-6}
150	all magnets max ΣB^2	2.2×10^{-4} (d)	.16	3.4×10^{-5}	1.7×10^{-5}
100	all magnets max ΣB^2	1.7×10^{-4} (c)	.56	1.0×10^{-4}	5×10^{-5}

(a) Pion decay before F4 is allowed for.

(b) With synchrotron radiation compensated settings.

(c) Hagedorn-Ranft model.

(d) Interpolated.

REFERENCES

1) J. F. Crawford, Z. G. T. Guiragossián, R. Hofstadter, E. B. Hughes R. E. Rand, R. F. Schilling, M. R. Yearian, E. V. Hungerford III, G. S. Mutchler, G. C. Phillips and B. W. Mayes, NAL Proposal No. 164.

2) J. J. Murray, (SLAC) private communication.

A. L. Read, (NAL) private communication.

D. D. Reeder (University of Wisconsin) private communication

3) General references on e beams at NAL

A. L. Read, Design Study, 200 BeV Accelerator, Vol. 1, UCRL-16830, 1966.

C. A. Heusch, Design Study, 200 BeV Accelerator Vol. 3, UCRL-16830, 1966.

W. T. Toner, 1968 NAL Summer Study, Vol. 2.

C. A. Heusch, Ibid.

R. Diebold and L. Hand, 1969 NAL Summer Study, Vol. 1.

C. A. Heusch, Ibid.

Z. G. T. Guiragossián and F. Villa, Ibid, Vol. 3 .

R. Morrison, K. Pretzl and A. L. Read, 1970 NAL Summer Study.

A. Mischke et al, Ibid.

R. Morrison et al, Proc. Int. Conf. on Instrumentation for H.E.P., Dubna, 1970.

A. L. Alikanian et al, IHEP 70-105, 1970. (Electron beam at Serpukhov)

4) This number is based on yield estimates calculated using a multiperipheral model (Ref. 7) and the Hagedorn-Ranft model, Suppl. Nuovo Cim. I, 6, 169, 1968.

5) C. Halliwell, P. J. Biggs, W. Busza, M. Chen, J. Nash, F. Murphy, G. Luxton and J. D. Prentice, Nuc. Inst. and Meth. 102, 51, 1972.

6) G. R. Charlton and G. H. Thomas, Phys. Letts., 40B, 378, 1972.

7) L. Caneschi and A. Pignotti, Phys. Rev. Letts., 22, 1219, 1969.

8) Particle Data Group, UCRL-20000 NN, August 1970.

9) D. Dekker et al, Phys. Rev. 137, B962, 1965.

10) W. Heitler, The Quantum Theory of Radiation, 3rd Ed., Oxford, 1954, p. 259 et seq.

11) K. L. Brown, SLAC-75.

12) TRANSPORT, K.L. Brown and S. K. Howry, SLAC-91.

13) TURTLE, D. Carey, NAL-64, 1971. F. Rothacker (SLAC) is to be thanked for assistance in running both programs, TRANSPORT and TURTLE.

14) T. Nash (NAL) private communication.

15) J. Cobb (SLAC) is to be thanked for providing this information and for elucidating the technique of the multipole expansion.

16) F. Murphy (UCSB) private communication.

17) B. Margolis, P. M. Patel, W. Ross, D. G. Stairs, L. Bird, C. Halliwell, R. Morrison, J. Walters, E. Coleman, T. Fesesse, Y. Makdisi, U. J. Becker, P. Biggs, W. Busza, M. Chen, T. Nash, H. F. W. Sadrozinski, S. C. C. Ting, S. L. Wu, T. T. Wu, NAL Proposal No. 144.

18) F. J. M. Farley, E. Picasso and L. Bracci, CERN NP Int. Rep. 71-11, 1971 and Nucl. Inst. and Meth. 103, 325, 1972.

19) P. J. Biggs (MIT) and J. Prentice (Univ. of Toronto) private communications.

FIGURE CAPTIONS

Fig. 1 Schematic Layout of Electron Beam.

Fig. 2 Electron yields calculated from a multiperipheral model[7] for the present beam line $(\Delta p/p)\ \Delta\Omega = 9.5\ \mu$ster % $\Delta p/p$, Beryllium target 40.3 cm, 0.5 rad. length lead radiator. Number of electrons/10^{13} incident protons at various production angles θ and momenta: (a) 200 GeV/c, (b) 300 GeV/c, (c) (c) 400 GeV/c, (d) 500 GeV/c, (e) 1000 GeV/c - See Text.

Fig. 3 Electron beam layout and optics.
(a) Arrangement of magnetic elements. Each symbol may represent several physical components as indicated. Positions of bending magnets and sextupoles are displaced where necessary for clarity. For exact locations see table II.
(b) First order matrix elements in horizontal (x) plane ($\delta = \Delta p/p$).
(c) First order matrix elements in vertical (y) plane.
(d) Second order beam envelopes as calculated by TRANSPORT[12] for $\Delta p/p = 0$ and $\pm$ 2% and primary aperture slits x = $\pm$ 15 mm and y = $\pm$ 30 mm.

Fig. 4 Vertical (y) beam profile ($\Delta p/p = \pm$ 3%) at first y focus ($F\frac{1}{2}$), showing size of slit for primary pion clean up. Histograms in figures 4-10 are calculated using the Monte Carlo ray tracing program TURTLE[13], based on effective primary spot size expected at 100 GeV/c. Effects of imperfections in the quadrupole fields, as actually measured[15] are taken into account. First order magnitudes as calculated by TRANSPORT[12] indicated where appropriate. Ordinate scales are linear and arbitrary.

Fig. 5. Momentum resolution and acceptance at F1.
(a) Resolution with sextupole adjusted to correct aberrations at F2. The slight asymmetry is due to the term $\langle x | x_o'\ x_o' \rangle$
(b) Resolution without sextupoles.
(c) Acceptance with sextupoles. Note the sharp cut off and the asymmetry.
(d) Acceptance without sextupoles.

Fig. 6 Beam profiles at F2.
(a) Horizontal profile with optimised sextupole settings. Note that the beam spot is almost entirely within the first order limits.
(b) Vertical profile. This occurs at a waist (not a focus) in the beam envelope and is unaffected by the sextupoles.
(c) Horizontal profile without sextupoles. The wings of this distribution would cause serious losses in subsequent stages.

Fig. 7 Momentum Resolution at F3 for primary beam spot ± 2.5 mm and no slit at F2. Resolution is shown for the nominal momentum p_o and for 1.016 p_o. The centroid displacements are due to the aberrations $\langle {}^{o}x|x_o'x_o'\rangle$ and $\langle x|\delta\delta\rangle$.

Fig. 8 Resolutions at angle hodoscopes.
(a) Horizontal (x) distributions for rays which pass through the experimental target at $\theta = 0$ and 0.5 mr. The finite distribution widths are mainly due to the small dispersion at the hodoscope, calculated for $\Delta p/p = \pm 2\%$.
(b) Vertical (y) distributions for rays which pass through the experimental target at $\phi = 0$ and 0.5 mr. The hodoscope cannot be located exactly at the primary vertical focus of the last quadrupole set, so that the finite widths are due to the vertical beam spot size.

Fig. 9 Electron beam profiles at experimental target focus [illegible] at 100 GeV/c.
(a) Horizontal (x)
(b) Vertical (y).

Fig. 10 Electron and pion horizontal beam profiles at F4 showing the effect of synchrotron radiation in a radiation compensated beam.
(a) 100 GeV/c, (b) 150 GeV/c. At these two momenta all the magnets in the beam line are used, some with reversed polarity, to maximize ΣB^2 and enhance the e, π separation.
(c) 200 GeV/c, (d) 300 GeV/c. At these higher momenta, only the necessary number of bending magnets consistent with $B \leq 14$ kgauss are used. See table II.

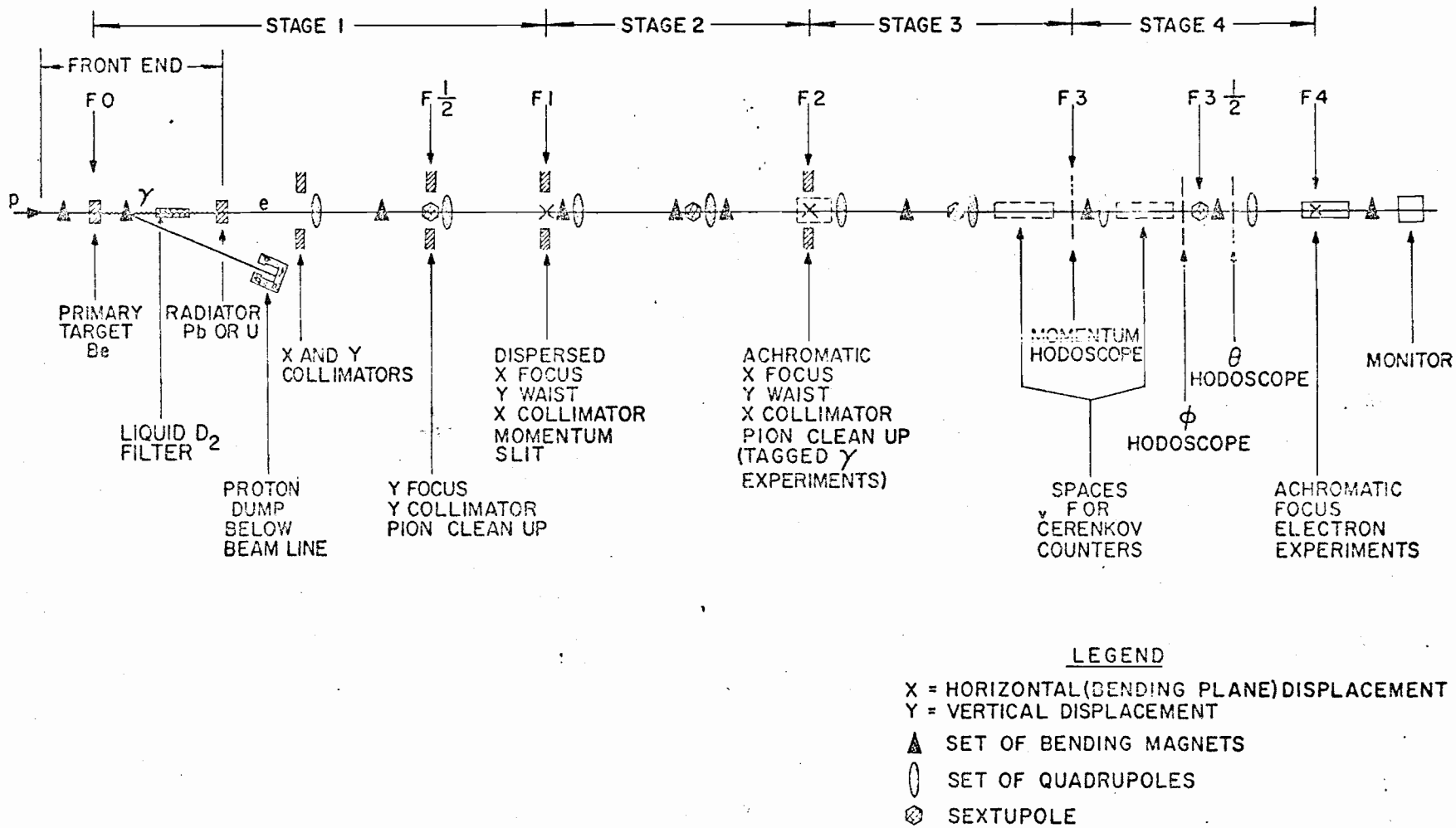

FIG. 1 SCHEMATIC LAYOUT OF ELECTRON BEAM

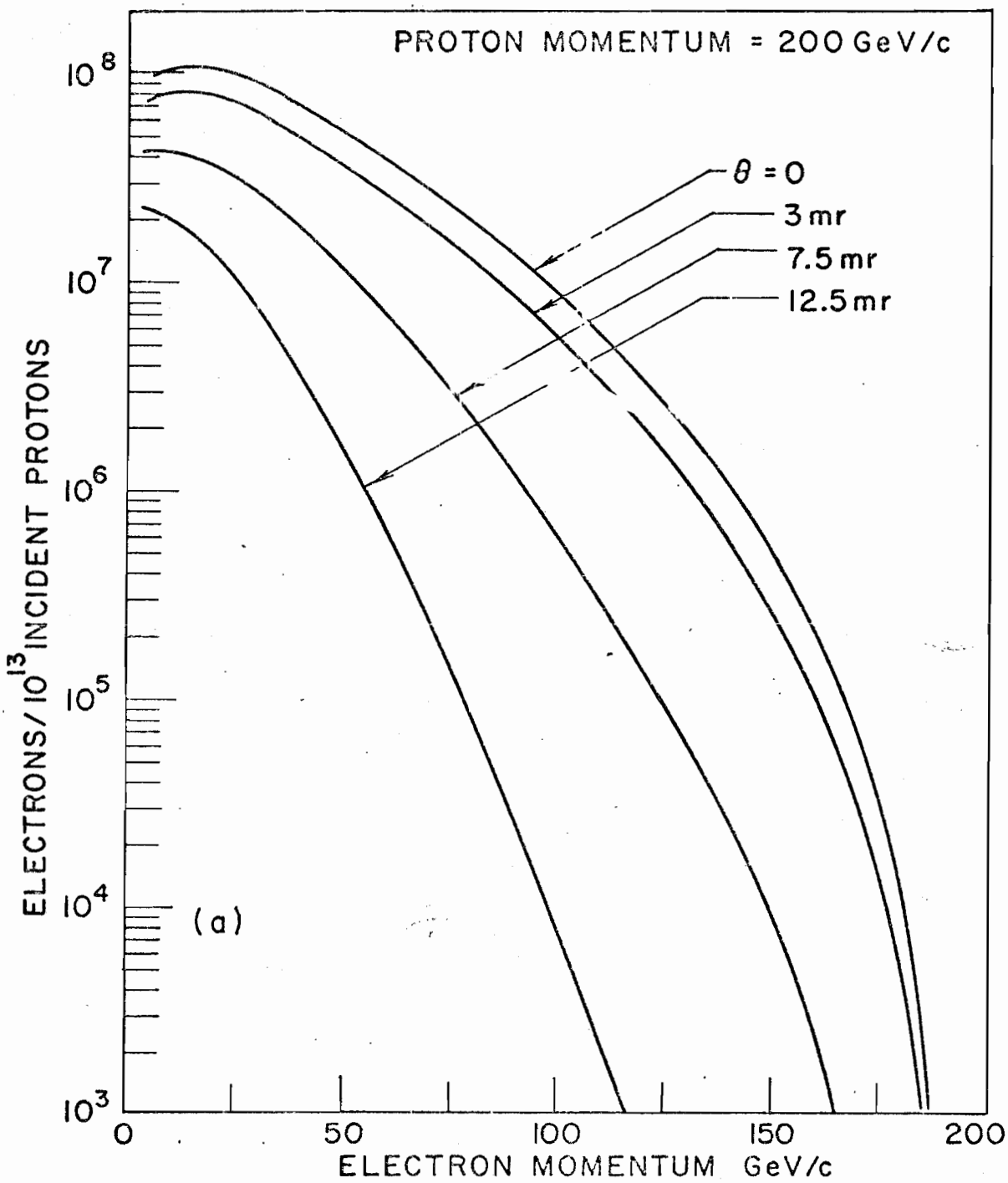
PROTON MOMENTUM = 200 GeV/c
θ = 0
3 mr
7.5 mr
12.5 mr
(a)
ELECTRONS/10^13 INCIDENT PROTONS
10^8
10^7
10^6
10^5
10^4
10^3
0
50
100
150
200
ELECTRON MOMENTUM GeV/c

FIG. 2(a)

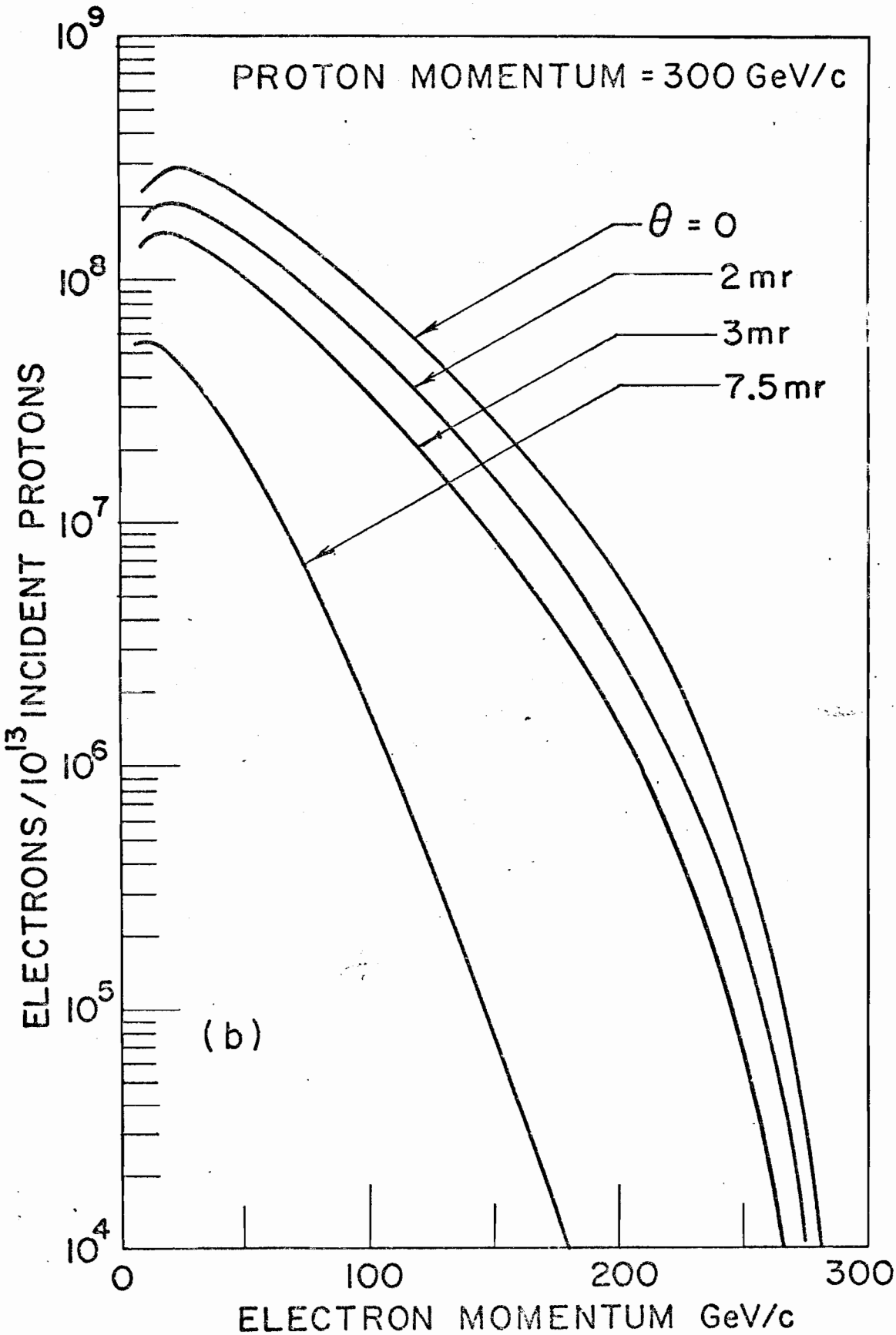
PROTON MOMENTUM = 300 GeV/c
θ = 0
2 mr
3mr
7.5 mr
(b)
ELECTRONS / 10^13 INCIDENT PROTONS
10^9
10^8
10^7
10^6
10^5
10^4
0
100
200
300
ELECTRON MOMENTUM GeV/c

FIG. 2(b)

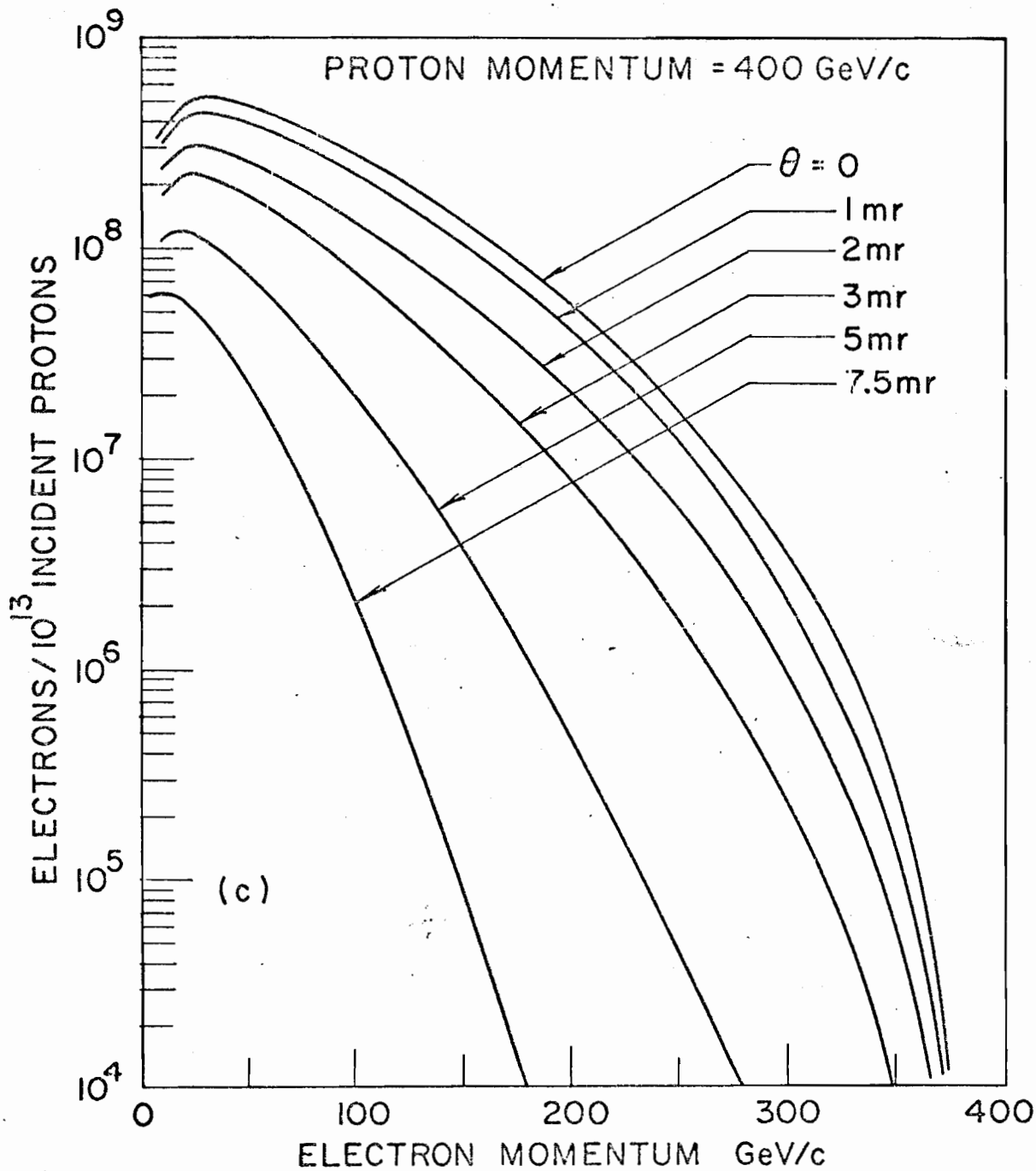
PROTON MOMENTUM = 400 GeV/c
θ = 0
1 mr
2 mr
3 mr
5 mr
7.5 mr
(c)
ELECTRONS/10^13 INCIDENT PROTONS
10^9
10^8
10^7
10^6
10^5
10^4
0
100
200
300
400
ELECTRON MOMENTUM GeV/c

FIG. 2(c)

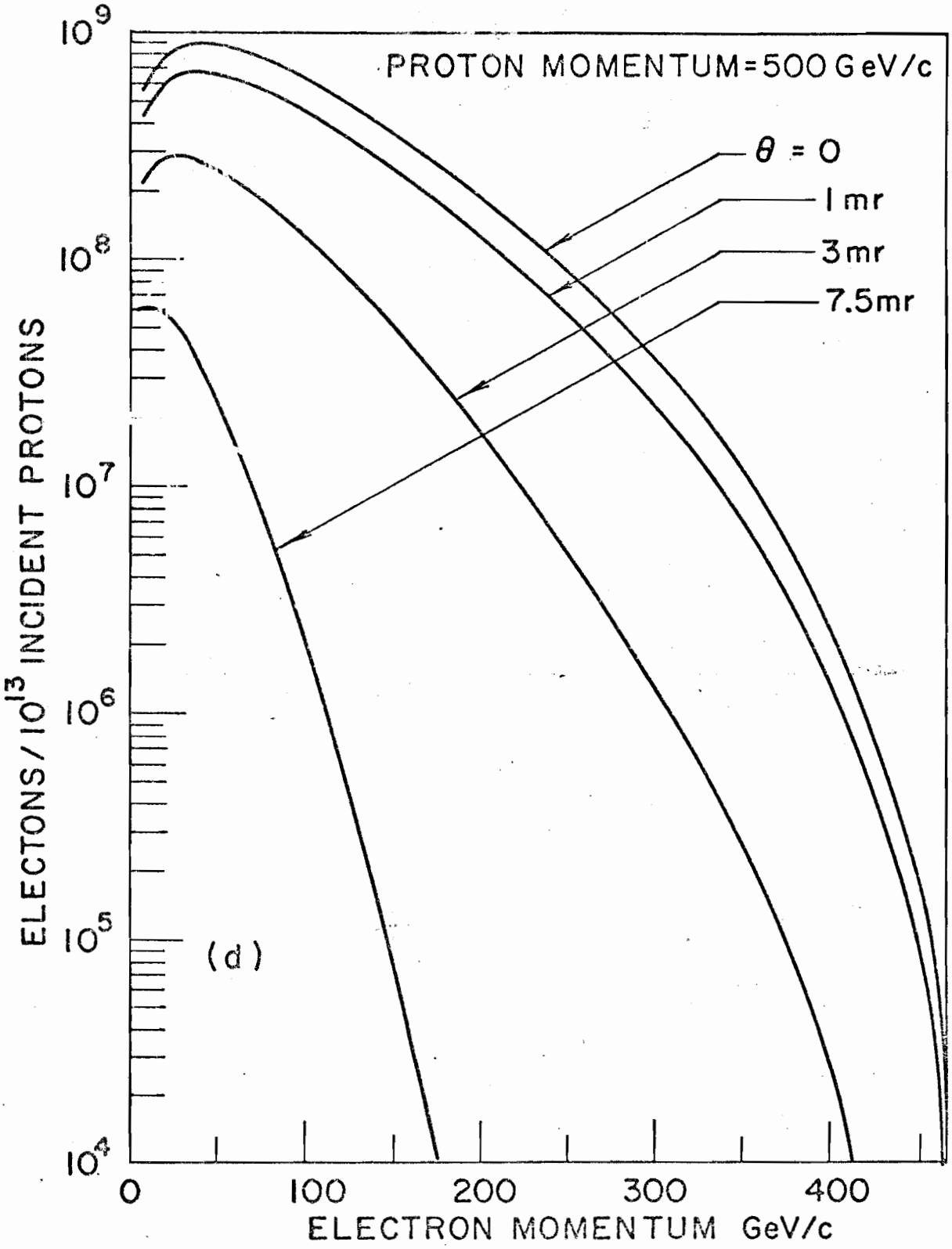
PROTON MOMENTUM=500 GeV/c
θ = 0
1 mr
3 mr
7.5mr
(d)
ELECTONS / 10^13 INCIDENT PROTONS
10^9
10^8
10^7
10^6
10^5
10^4
0
100
200
300
400
ELECTRON MOMENTUM GeV/c

FIG. 2(d)

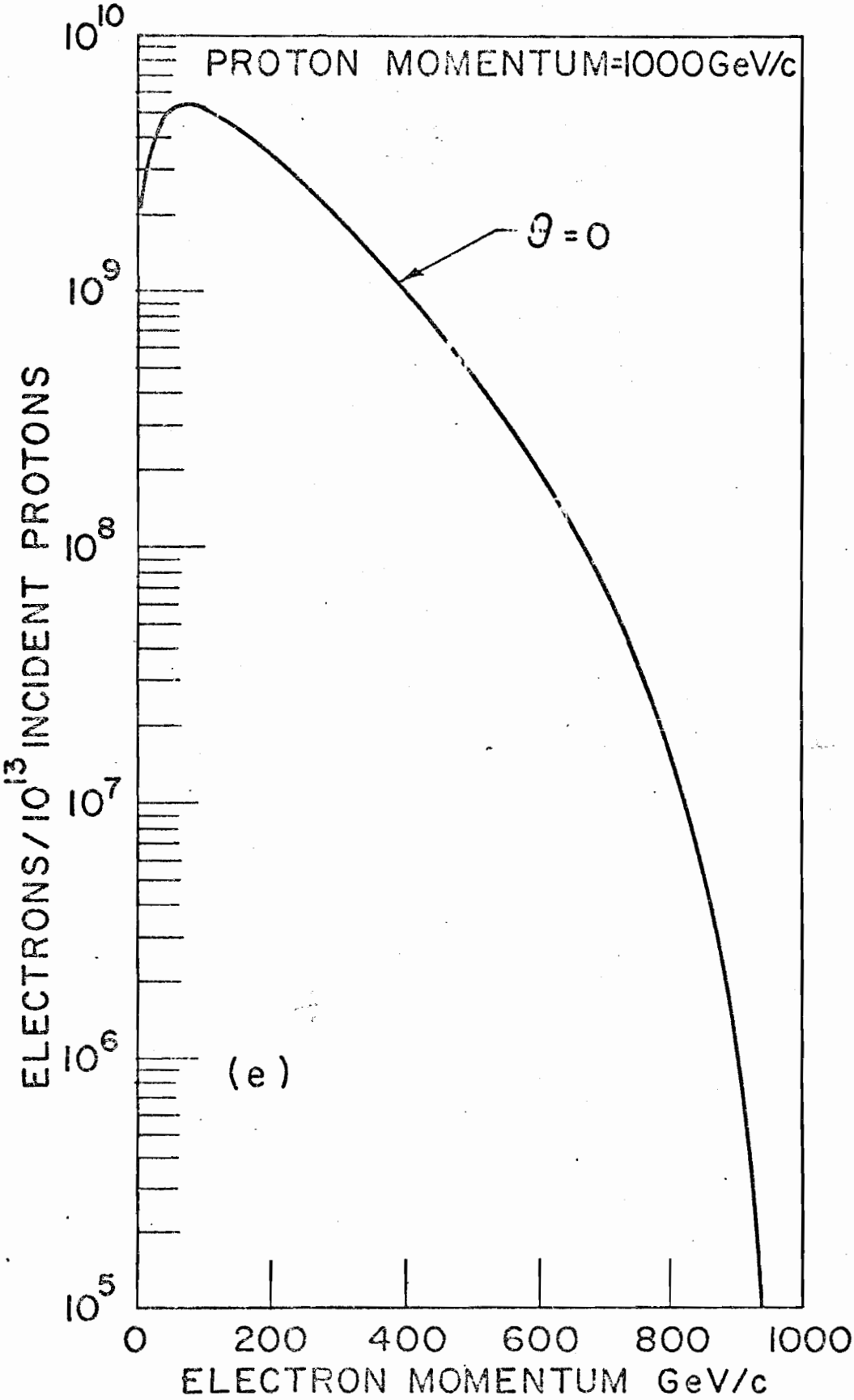
PROTON MOMENTUM=1000GeV/c
$\theta = 0$
(e)
10^{10}
10^{9}
10^{8}
10^{7}
10^{6}
10^{5}
ELECTRONS/10^{13} INCIDENT PROTONS
0
200
400
600
800
1000
ELECTRON MOMENTUM GeV/c

FIG. 2(e)

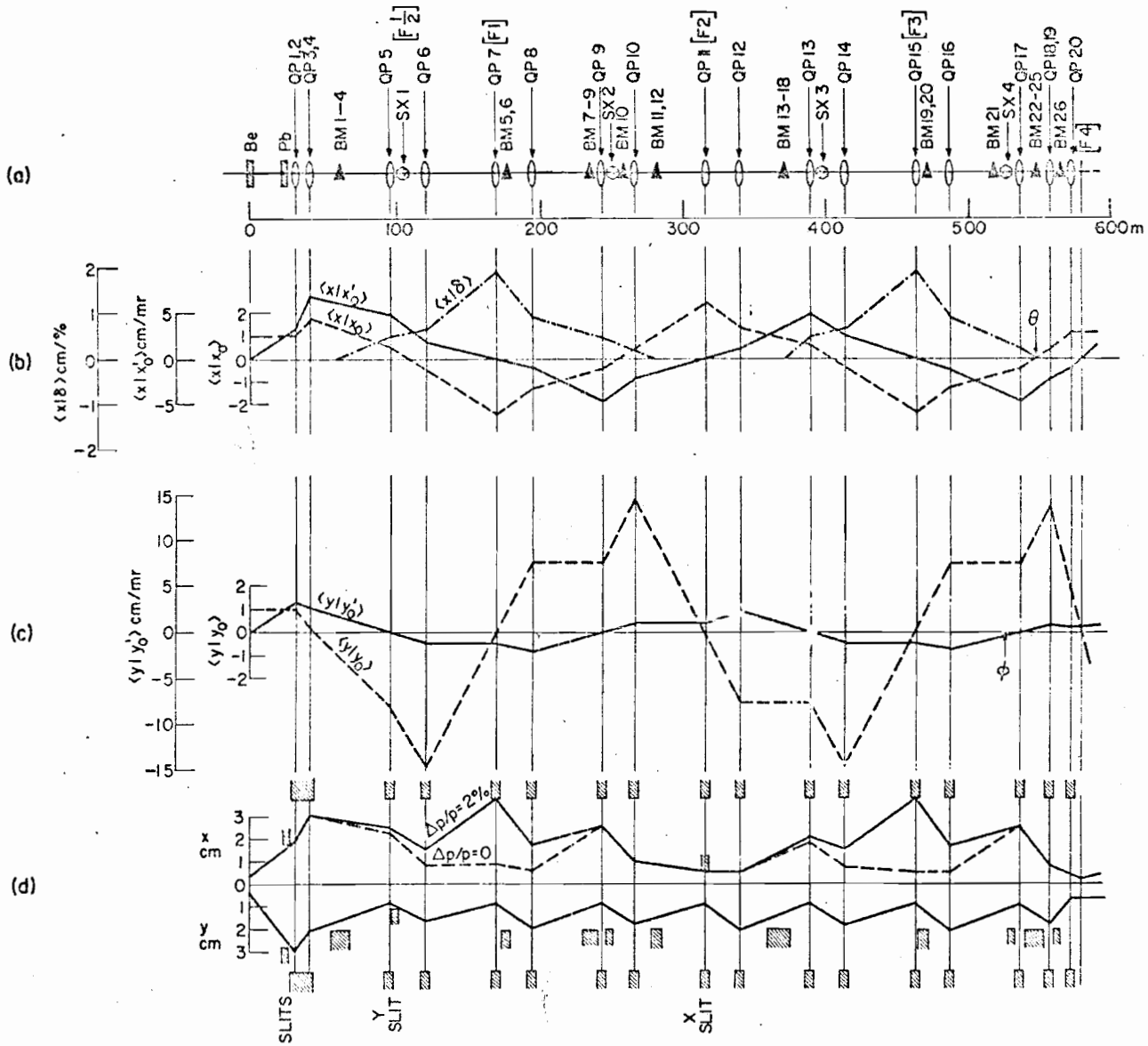

FIG. 3 ELECRON BEAM LAYOUT AND OPTICS

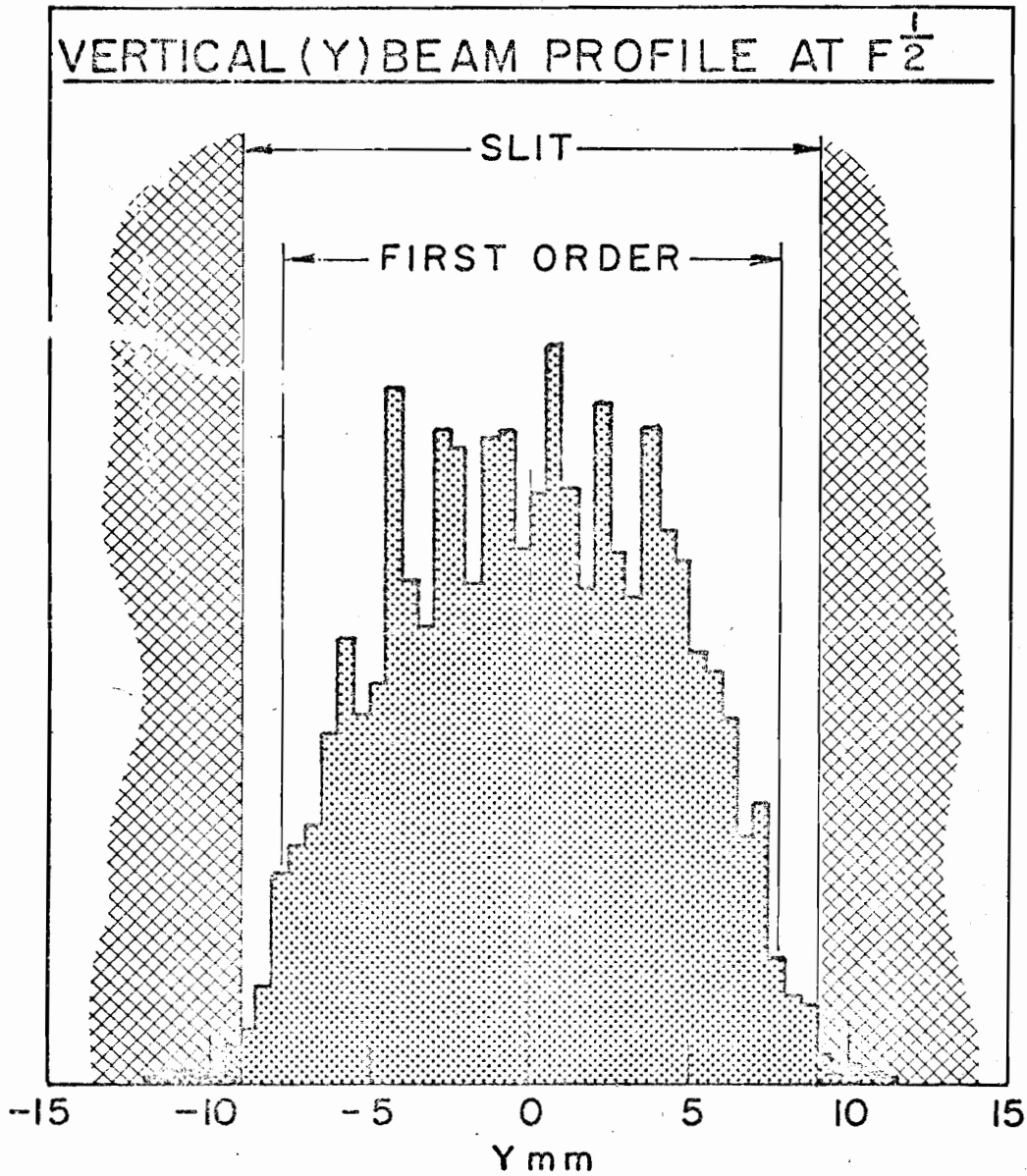
VERTICAL (Y) BEAM PROFILE AT F 1/2
SLIT
FIRST ORDER
-15
-10
-5
0
5
10
15
Y mm

FIG. 4

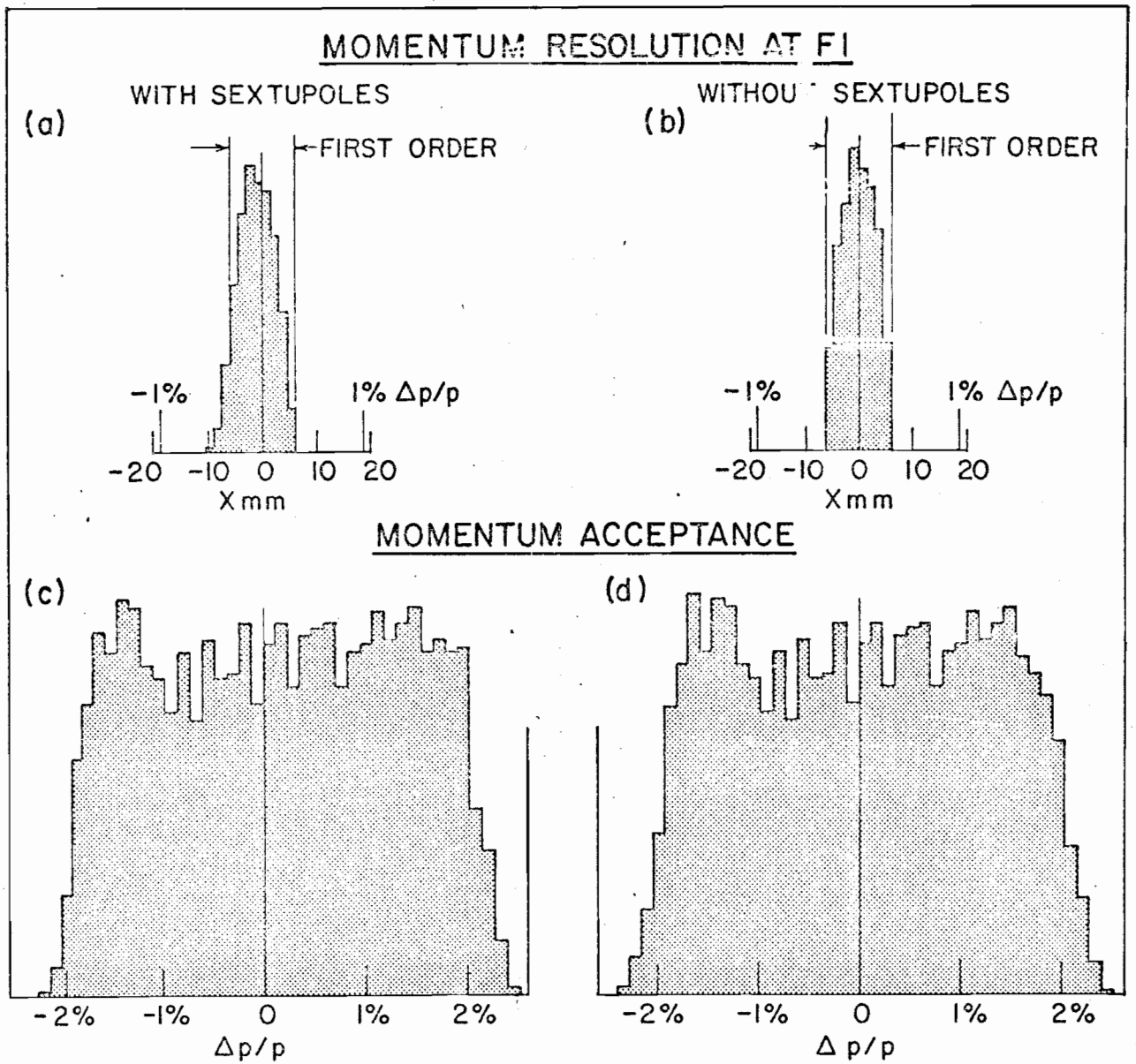
MOMENTUM RESOLUTION AT F1
(a)
WITH SEXTUPOLES
FIRST ORDER
-1%
1% Δp/p
-20 -10 0 10 20
X mm
(b)
WITHOUT SEXTUPOLES
FIRST ORDER
-1%
1% Δp/p
-20 -10 0 10 20
X mm
MOMENTUM ACCEPTANCE
(c)
-2% -1% 0 1% 2%
Δp/p
(d)
-2% -1% 0 1% 2%
Δ p/p

FIG. 5

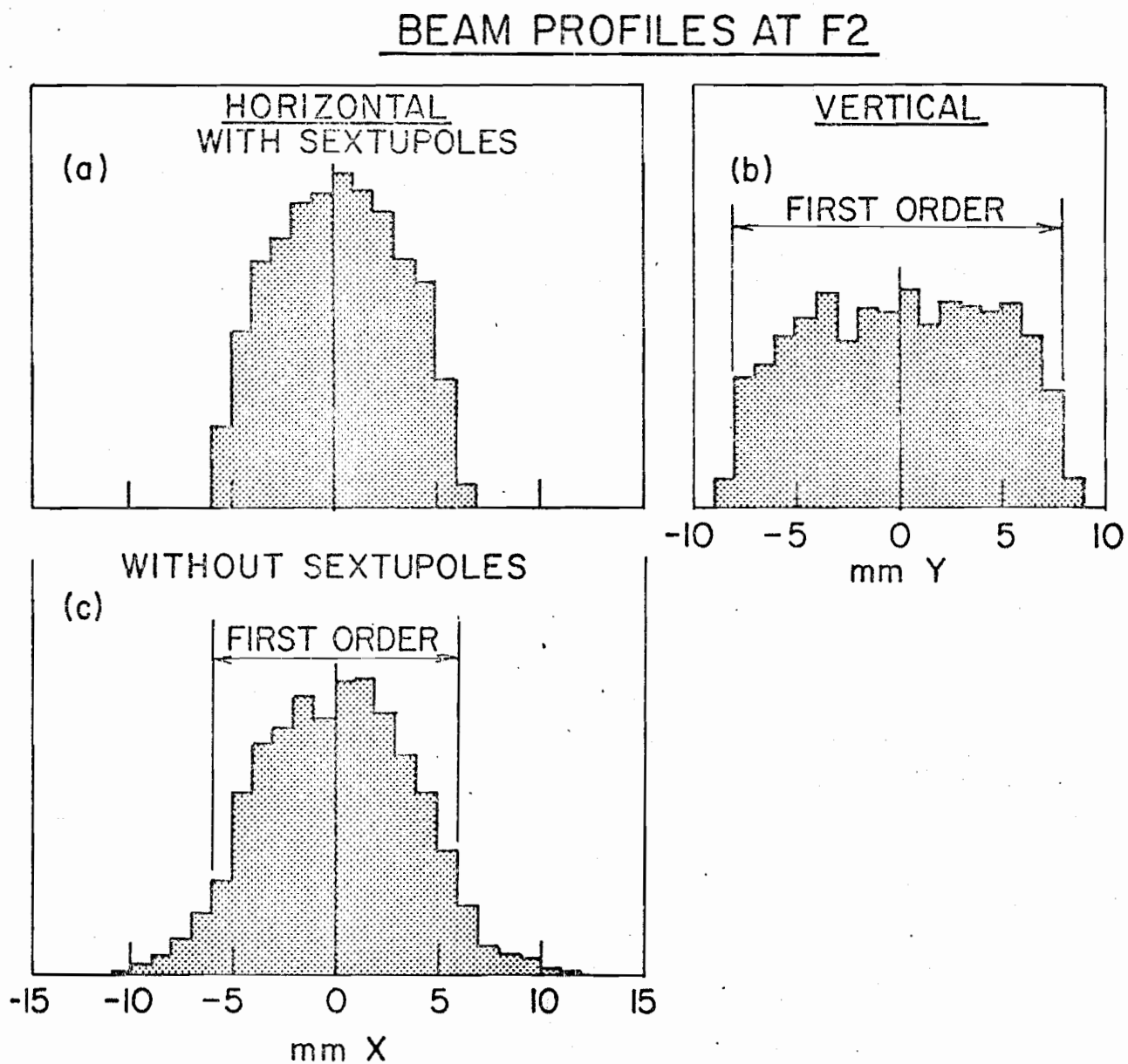
BEAM PROFILES AT F2
HORIZONTAL
WITH SEXTUPOLES
(a)
VERTICAL
(b)
FIRST ORDER
-10
-5
0
5
10
mm Y
WITHOUT SEXTUPOLES
(c)
FIRST ORDER
-15
-10
-5
0
5
10
15
mm X

FIG. 6

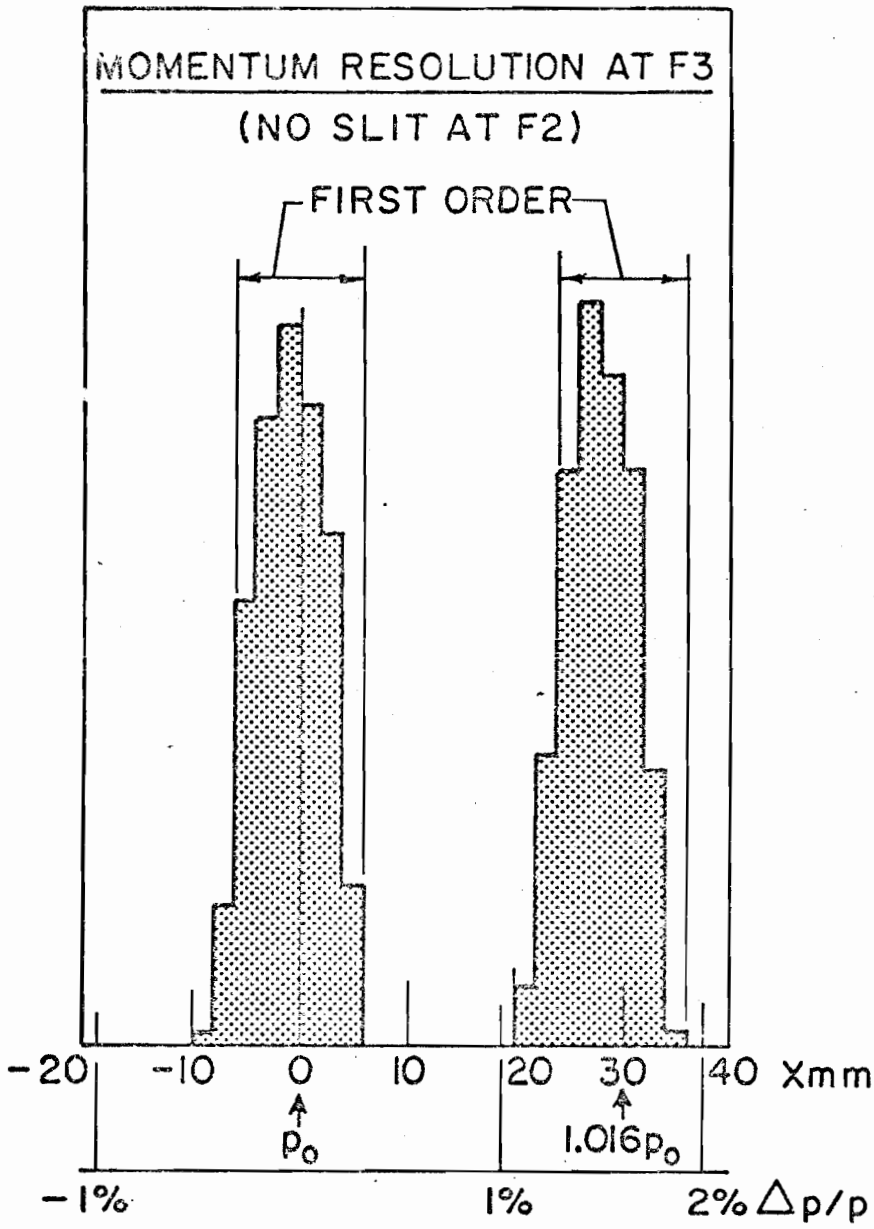
MOMENTUM RESOLUTION AT F3
(NO SLIT AT F2)
FIRST ORDER
-20
-10
0
10
20
30
40
Xmm
p_o
$1.016p_o$
-1%
1%
2%
$\Delta p/p$

FIG. 7

RESOLUTION AT ANGLE HODOSCOPES

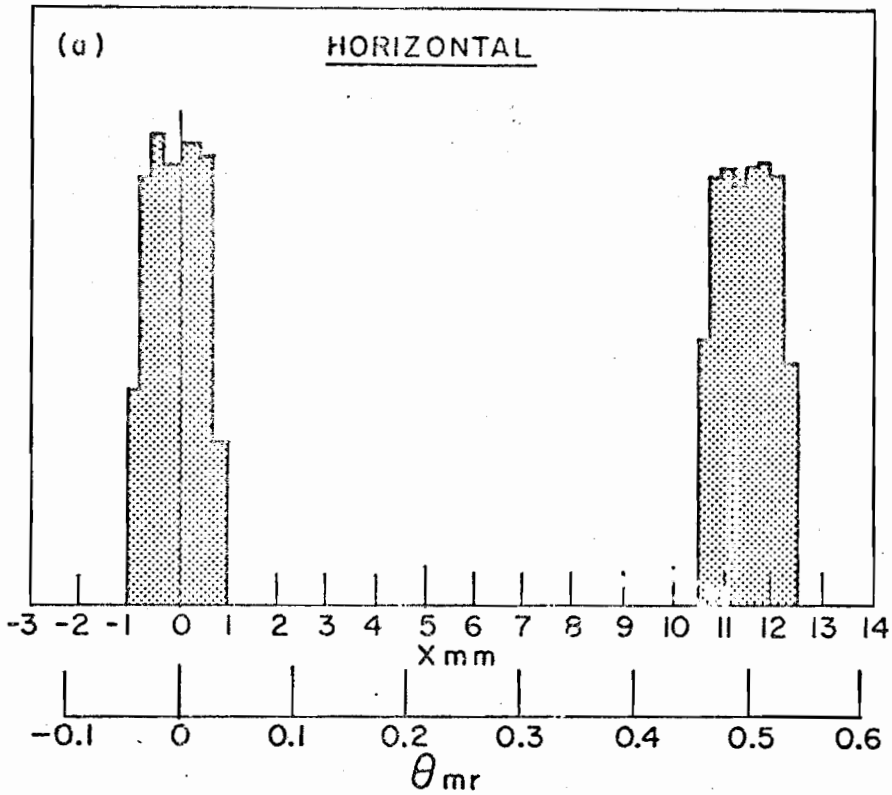

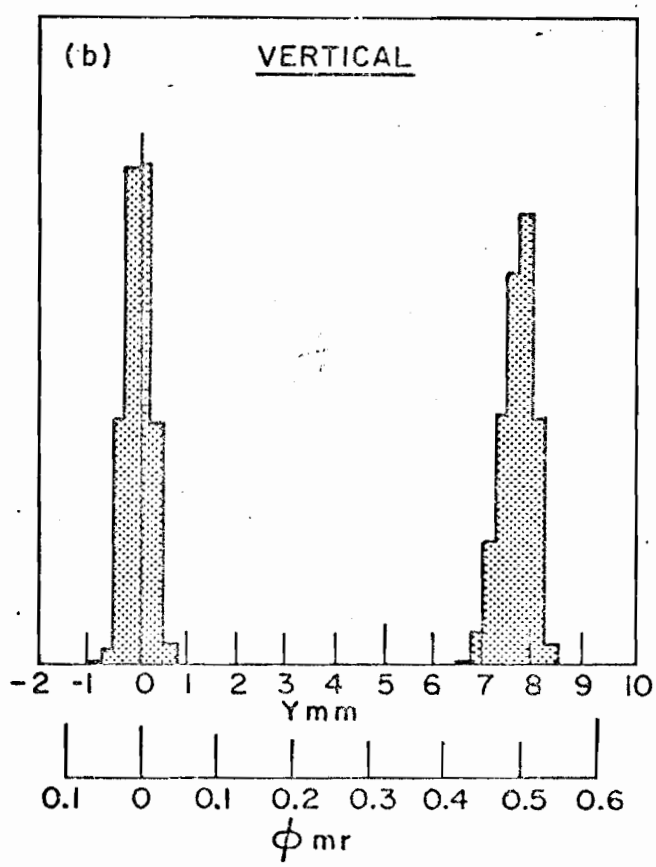

FIG. 8

BEAM PROFILES AT F4 AT 100 GeV/C

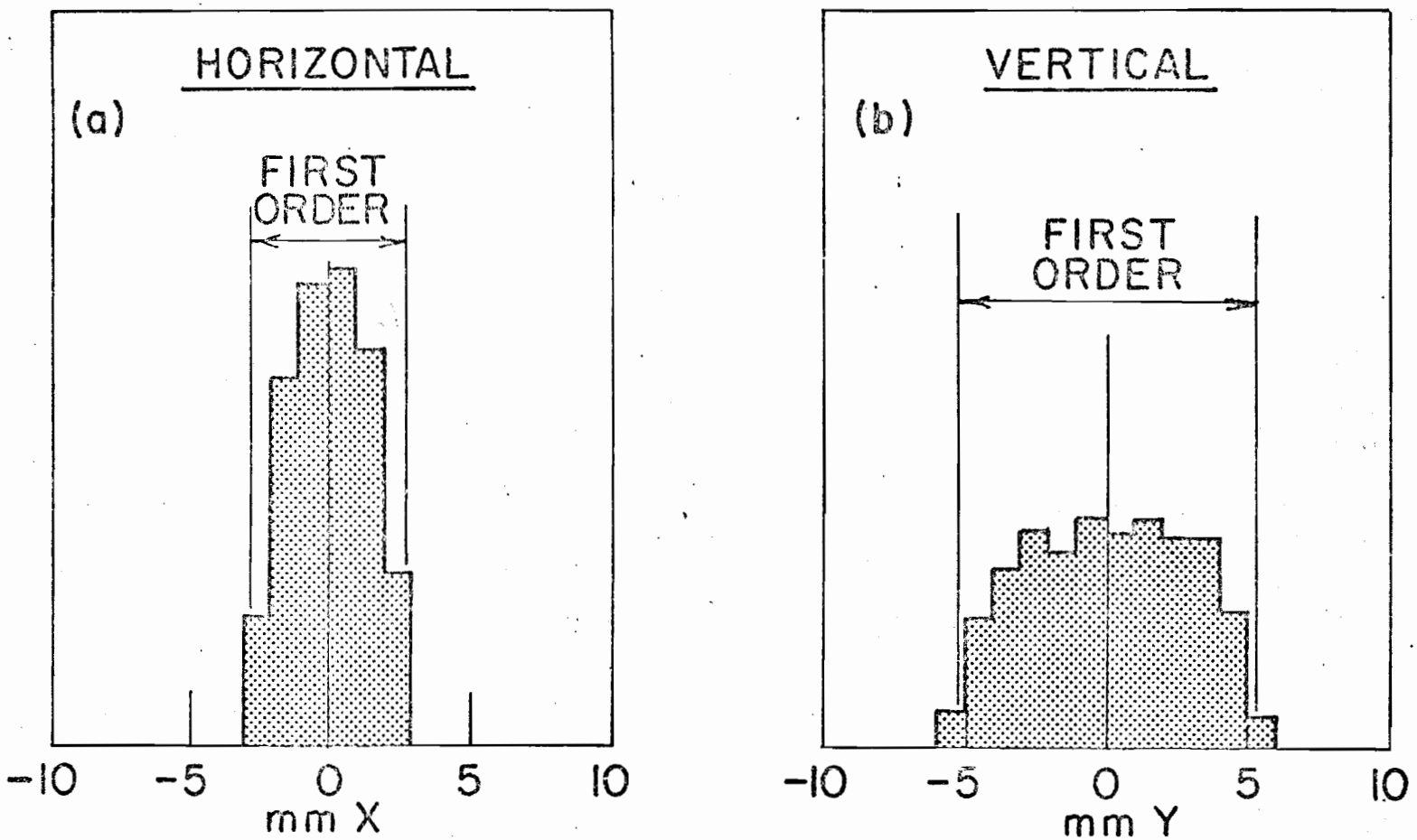

FIG. 9

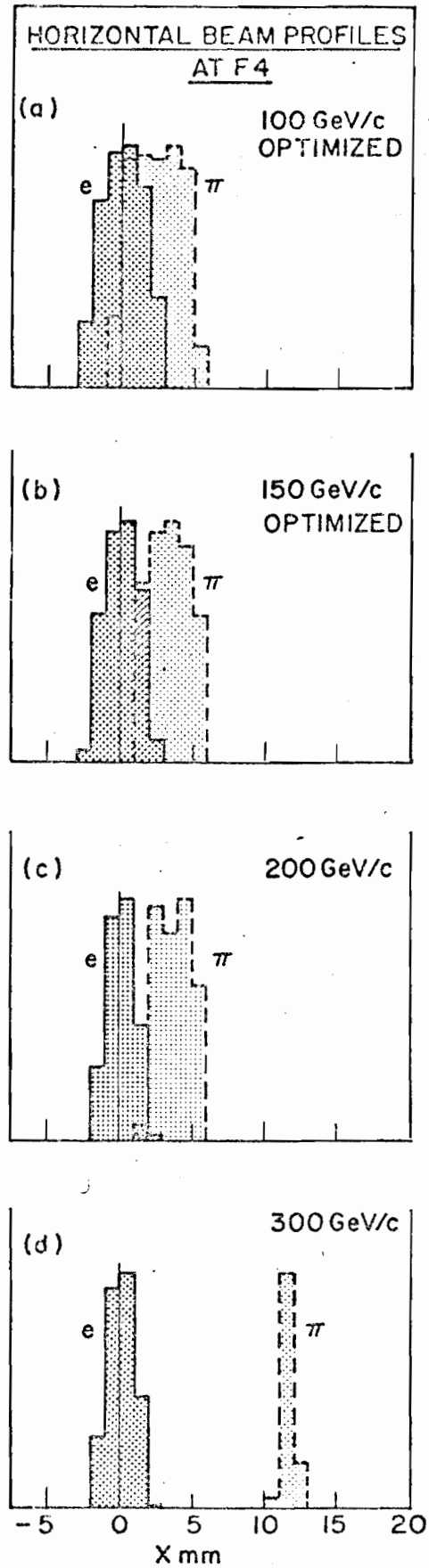
HORIZONTAL BEAM PROFILES
AT F4
(a)
100 GeV/c
OPTIMIZED
e
π
(b)
150 GeV/c
OPTIMIZED
e
π
(c)
200 GeV/c
e
π
(d)
300 GeV/c
e
π
-5
0
5
10
15
20
X mm

FIG. 10